Research Article | Vol. 25, No. 24 | 27 Nov 2017 | OPTICS EXPRESS 30642

Optics EXPRESS

Structured light illumination for order sorting in Echelle spectrometers

Ó. MARTÍNEZ-MATOS,[1,*] P. VAVELIUK,[2] AND C. RICKENSTORFF[1]

[1] *Departamento de Óptica, Facultad de Ciencias Físicas, Universidad Complutense de Madrid, 28040, Madrid, Spain*

[2] *Centro de Investigaciones Opticas (CONICET La Plata-CIC), Cno. Centenario y 506, P.O. Box 3, 1897 Gonnet, Argentina*

[*] *omartine@fis.ucm.es*

Abstract: We report on the operation of an echelle spectrometer under structured light illumination. Each diffraction order of the spectrometer is encoded with a certain periodic structure allowing for order sorting by numerical analysis after detection. In contrast to cross-dispersed echelle spectrometers, in this approach the orders overlap at the detection plane so that the spectral calibration can be performed easily with a single reference wavelength. This operational simplification makes it possible to measure simultaneously the light source under study and the calibration wavelength giving rise to a self-calibrated echelle spectrometer. In this way the device compensates for the spectral drift due to temporal changes of environmental conditions in real time. Our proposal can be useful in a large number of applications requiring moderate, high or very high resolving power for a wide bandwidth in a non-isolated environment.

OCIS codes: (300.6190) Spectrometers; (120.6200) Spectrometers and spectroscopic instrumentation; (070.4790) Spectrum analysis; (120.3180) Interferometry.

References and links

1. M. Mayor, F. Pepe, D. Queloz, F. Bouchy, G. Rupprecht, G. Lo Curto, G. Avila, W. Benz, J.-L. Bertaux, X. Bonfils, T. Dall, H. Dekker, B. Delabre, W. Eckert, M. Fleury, A. Gilliotte, D. Gojak, J. C. Guzman, D. Kohler, J.-L. Lizon, A. Longinotti, C. Lovis, D. Megevand, L. Pasquini, J. Reyes, J.-P. Sivan, D. Sosnowska, R. Soto, S. Udry, A. van Kesteren, L. Weber, and U. Weilenmann, "Setting New Standards with HARPS," The Messenger **114**, 20–24 (2003).
2. M. R. Patel, P. Antoine, J. Mason, M. Leese, B. Hathi, A. H. Stevens, D. Dawson, J. Gow, T. Ringrose, J. Holmes, S. R. Lewis, D. Beghuin, P. van Donink, R. Ligot, J.-L. Dewandel, D. Hu, D. Bates, R. Cole, R. Drummond, I. R. Thomas, C. Depiesse, E. Neefs, E. Equeter, B. Ristic, S. Berkenbosch, D. Bolsée, Y. Willame, A. C. Vandaele, S. Lesschaeve, L. D. Vos, N. V. Vooren, T. Thibert, E. Mazy, J. Rodriguez-Gomez, R. Morales, G. P. Candini, M. C. Pastor-Morales, R. Sanz, B. A. del Moral, J.-M. Jeronimo-Zafra, J. M. Gómez-López, G. Alonso-Rodrigo, I. Pérez-Grande, J. Cubas, A. M. Gomez-Sanjuan, F. Navarro-Medina, A. BenMoussa, B. Giordanengo, S. Gissot, G. Bellucci, and J. J. Lopez-Moreno, "Nomad spectrometer on the exomars trace gas orbiter mission: part 2—design, manufacturing, and testing of the ultraviolet and visible channel," Appl. Opt. **56**, 2771–2782 (2017).
3. A. Baranne, D. Queloz, M. Mayor, G. Adrianzyk, G. Knispel, D. Kohler, D. Lacroix, J.-P. Meunier, J.-P. G. Rimbaud, and A. Vin, "Elodie: A spectrograph for accurate radial velocity measurements," Astron. Astrophys. Suppl. Ser. **119**, 373–390 (1996).
4. R. P. Butler, G. W. Marcy, E. Williams, C. McCarthy, P. Dosanjh, and S. S. Vogt, "Attaining doppler precision of 3 m s-1," Publications of the Astronomical Society of the Pacific **108**, 500 (1996).
5. A. Reiners, R. K. Banyal, and R. G. Ulbrich, "A laser-lock concept to reach cm s-1 precision in Doppler experiments with Fabry-Perot wavelength calibrators," AA **569**, A77 (2014).
6. M. T. Murphy, T. Udem, R. Holzwarth, A. Sizmann, L. Pasquini, C. Araujo-Hauck, H. Dekker, S. D'Odorico, M. Fischer, T. W. Hansch, and A. Manescau, "High-precision wavelength calibration of astronomical spectrographs with laser frequency combs," Monthly Notices of the Royal Astronomical Society **380**, 839 (2007).
7. N. G. Douglas, "Heterodyned holographic spectroscopy," Publications of the Astronomical Society of the Pacific **109**, 151–165 (1997).
8. J. E. Lawler, Z. E. Labby, J. M. Harlander, and F. L. Roesler, "Broadband, high-resolution spatial heterodyne spectrometer," Appl. Opt. **47**, 6371–6384 (2008).
9. D. J. Erskine, "An externally dispersed interferometer prototype for sensitive radial velocimetry: Theory and demonstration on sunlight," Publications of the Astronomical Society of the Pacific **115**, 255 (2003).
10. O. Martínez-Matos, C. Rickenstorff, S. Zamora, J. Izquierdo, and P. Vaveliuk, "Characterization of digital dispersive spectrometers by low coherence interferometry," Opt. Express **25**, 3222–3233 (2017).

#302377 https://doi.org/10.1364/OE.25.030642
Journal © 2017 Received 14 Jul 2017; revised 31 Oct 2017; accepted 31 Oct 2017; published 22 Nov 2017

Optics EXPRESS

11. J. C. van Eyken, J. Ge, and S. Mahadevan, "Theory of dispersed fixed-delay interferometry for radial velocity exoplanet searches," The Astrophysical Journal Supplement Series **189**, 156 (2010).
12. "National institute of standards and technology: http://physics.nist.gov/physrefdata/handbook/tables," .
13. J. Fisher, M. M. Baumback, J. H. Bowles, J. M. Grossmann, and J. A. Antoniades, "Comparison of low-cost hyperspectral sensors," in *Imaging Spectrometry IV* (SPIE, 1998).

1. Introduction

Very fine spectral analysis of light possessing a wide bandwidth is customary performed with echelle spectrometers (ES). Their uncountable applications cover a wide field of scientific investigations in laser induced breakdown spectroscopy, Raman and fluorescence spectroscopy and exoplanet search by the radial velocity method to name a few. The dispersive element of the ES is the echelle grating, which is specially designed for use in high diffraction orders allowing for increased dispersion and high resolving power. However, the enlarged resolution comes at the expense of order (channel) overlapping at the detection plane. Consequently, a method for order sorting is needed to extract the spectrum without ambiguity and to provide a broad operation range given by the spectral contribution from all available channels. The most used method for channel sorting employs a crossed low-dispersion element (grating or prism) to map all the channels simultaneously onto the detection plane in different spatial locations. A representative instrument of this kind is the HARPS spectrograph used for exoplanet search [1]. An alternative separation method filters the incident spectrum to activate a single channel on each measurement by an acousto-optic tunable filter [2]. Although this last option also offers high resolving capabilities it is more time consuming since each channel is measured independently. The search of new methods for order sorting could bring novel devices with improved characteristics.

The wavelength calibration of the ES is a very critical task that requires a precise assignment pixel-wavelength to all the spectrometer channels. The most used calibration techniques employs emission lamps [3], gas absorption cells [4], Fabry-Perot interferometer-based calibrators [5] and laser frequency combs [6]. Once the spectrometer is carefully calibrated it must be pressure and temperature stabilized to avoid spectral drifts due to temporal changes of environmental conditions. Unfortunately, spectrometer stabilization and maintenance is a cumbersome task and increase substantially its price. An affordable alternative is a spectrometer capable to perform a self-calibration in every spectral measurement for a proper spectral drift correction. However, its realization is very complex due to the high number of spectral lines needed to cover all the spectrometer channels. It remains a challenge to find a simple method for ES calibration suitable to be implemented in every spectral measurement.

In this work we codify a certain periodic structure to each order of the ES by illuminating it with structured light. Contrary to traditional cross-dispersed ES, the orders overlap spatially at the detection plane with a different period being possible to sort them numerically by means of a Fourier transformation. Our approach features simultaneously multi-channel measurement, as in conventional cross-dispersed ES, by using a single reference wavelength for its calibration. The spectrometer is self-calibrated in every spectrum analysis compensating for the spectral drift due to environmental conditions. The performance of our method is demonstrated by implementing a self-calibrated and non-isolated high resolving power ES ($R \sim 5000 - 7000$) with a broad wavelength operational range ($400\,nm - 850\,nm$).

2. Experimental setup

The approach is composed by two parts as illustrated in Fig. 1. On the right the ES in the Czerny-Turner configuration is schematically presented. This is a 4f system consisting on a vertical slit (y-axis) on the input plane, an echelle grating on the Fourier Plane and a camera (CCD, Imaging Source, 8-bit gray level, 1280×960 pixels, pixel size $4.65\,\mu m$) on the Image Plane. The ES images the slit at the camera at different horizontal positions x depending on the

Optics EXPRESS

wavelength. Since the echelle grating is blazed for use in high diffraction orders, multiple orders overlap at the CCD mixing the spectral information (for simplicity Fig. 1 shows the behavior of a single order). This unwanted effect is solved by illuminating the input slit with structured light consisting on a periodic spatial structure along the slit axis with a wavelength dependent period. The total intensity at position x on the CCD is the addition of one intensity pattern per order possessing different periods. Thereby the channels are separated in the reciprocal space Fourier transforming the signal along the y-axis.

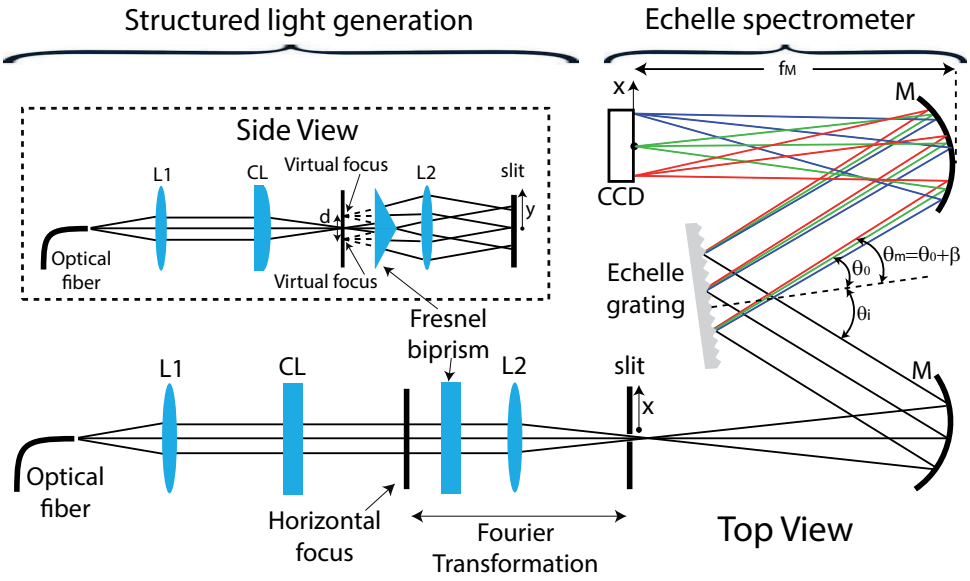

Fig. 1. Experimental setup. Left side: optical system to produce the structured light. Right side: echelle spectrometer in the Czerny-Turner configuration. L1, L2, CL and M: spherical lenses 1 and 2, cylindrical lens and mirrors, with focal lengths $f_1 = 25\,cm$, $f_2 = 20\,cm$, $f_{CL} = 10\,cm$ and $f_M = 10\,cm$, respectively. The Fresnel biprism has an apex angle of 0.7 degrees. The echelle grating is $25\,mm \times 50\,mm$ size, 63 blaze and has 79 $grooves/mm$.

The left side of Fig. 1 shows the setup to obtain the structured light. The light coming from an optical fiber is collimated by lens L1 and focused on the horizontal axis (x-axis) by the cylindrical lens CL. Two parallel virtual foci on x-axis are created by the Fresnel biprism (see the inset of Fig. 1) and the optical Fourier transform of this plane is performed by lens L2. The output signal is the interference of light coming from the virtual foci yielding a wavelength-dependent periodic structure along the y-axis that match the input slit of the ES. The figure caption list the parameter values of the optical elements. A Michelson interferometer can also be used to obtain the structured light instead of the Fresnel biprism. In fact, the combination of interferometry and dispersion for spectral analysis has been exploited in Heterodyned Holographic Spectrometer [7] and in Spatial Heterodyne Spectrometer [8] in which the mirrors of a Michelson interferometer are substituted by diffraction gratings. In these configurations the resolving capabilities of the devices are defined by the Fourier transformation of the signal in the same manner that in Fourier transform spectroscopy. Furthermore, several types of spectrometers composed by a Michelson interferometer to create an interference pattern and a dispersion spectrometer to separate the spectrum in smaller bandwidths have been reported [9–11]. The resolving capabilities of these devices are achieved by the Moire effect [9], by the fringes at the spectrum [11] or by a Fourier transformation as well [10]. However, to the best of our knowledge, structured illumination is used for order sorting in ES for first time. The resolving power is solely determined by the

Optics EXPRESS

echelle spectrometer while the Fourier transformation is exclusively used for order sorting. This operational principle presents a great advantage since the channels overlap at the camera, which is the key for performing the self-calibration process as we will discuss below. Also, the requirements on the interference pattern to sort the channels are much less stringent than in Fourier transform spectroscopy, relaxing the isolation constrains of our structured light generator.

3. Theory

The foundation of our proposal is described in this section. The grating equation

$$\sin\theta_m + \sin\theta_i = m\frac{c}{\Lambda\nu}, \tag{1}$$

relates the incidence, θ_i, and diffracted, θ_m, angles of light with frequency ν and order m to the grating period Λ of the echelle grating. Parameter c is the speed of light in vacuum. The ES is designed such that light with frequency ν_0 and order m_0 impinges at the center of the CCD after been diffracted by an angle θ_0. Then, the diffracted angle of m-order can be measured from θ_0 as $\theta_m = \theta_0 + \beta$, see Fig. 1, where $\beta \ll \theta_0$ if the echelle grating is used in high diffraction orders. Taking this fact into account, the frequency in (1) can be written as

$$\nu(x,m) \sim \frac{c}{\Lambda}(A + B\,x)\,m, \tag{2}$$

where a Taylor series up to the first order in β has been performed, and it has been used the relation $\sin\theta_0 + \sin\theta_i = m_0\lambda_0/\Lambda$ derived from (1) for $\theta_m = \theta_0$. The parameters in (2) are $A = \Lambda/(m_0\lambda_0)$ and $B = -A^2\cos\theta_0/f_M$, being the CCD spatial coordinate along the dispersion axis defined as $x = f_M\beta$, where f_M is the focal length of the spherical mirrors M, see Fig. 1. The signal, Γ, recorded by the camera is the addition of one intensity pattern by each diffraction order:

$$\Gamma(x,y) = \text{rect}\left(\frac{x}{a}\right)\text{rect}\left(\frac{y}{b}\right)\sum_m I[\nu(x,m)]\left\{1 + \cos\left[\pi\frac{d}{f_2\Lambda}(A + B\,x)\,m\,y\right]\right\}, \tag{3}$$

where the summation limits cover all the orders m (channels in the CCD) that impinge on the camera. The rect function is the usual rectangular function, a and b are the horizontal and vertical dimensions of the CCD chip, $I[\nu(x,m)]$ is the spectral intensity of the light source, d the distance between the two virtual horizontal foci (see the inset of Fig. 1) and f_2 the focal length of lens L2. Expression (3) shows that the total intensity at x is the addition of intensity patterns, each one from a different order possessing a different period. The periodic functions along the y-axis are due to the structured illumination, which is the key to order sorting.

The order sorting can be obtained from signal (3) performing the Fourier transformation along the y-axis for each position x:

$$\widehat{\Gamma}(x,u) = b\,\text{rect}\left(\frac{x}{a}\right)\sum_m I[\nu(x,m)]\,\frac{\sin\left\{\pi\,b\left[u - \frac{d}{2f_2\Lambda}(A + B\,x)\,m\right]\right\}}{\pi\,b\left[u - \frac{d}{2f_2\Lambda}(A + B\,x)\,m\right]}, \tag{4}$$

where y and u are conjugate variables. It can be seen that the channels are sinc functions located at different positions along u. Each sinc function is weighted by an specific portion of the spectral intensity, therefore, the whole spectrum is extracted from (4) in the reciprocal space by just measuring the sinc amplitudes. Equations (3) and (4) show the effect of overlapping channels on the CCD, but doesn't describes the full optical capabilities of the ES. In fact, to obtain (4) three assumptions were considered: an ideal interference pattern visibility, a thin slit and a non-aberrated ES. In practice, maximum fringe visibility is achieved when the horizontal focus have a width less than 40 μm. This can be obtained either by a proper combination of focal

Optics EXPRESS

lengths and apertures of L1 and CL or reducing the focal width with an horizontal slit at the focal plane of the CL.

The design of the present proposal yields a very simple calibration method using a single reference wavelength. The calibration method is based on two hypothesis. The first one states that wavelengths from different orders that impinge the camera at the same pixel x are diffracted by the echelle grating at the same angle. From this property and using (1), it is possible to know one wavelength per order at x. This means that, providing the position x_0 of a reference wavelength $\lambda_{m_0}^{x_0}$ of order m_0, the wavelength $\lambda_m^{x_0}$ of order m at x_0 is known as:

$$\lambda_m^{x_0} = \frac{m_0}{m}\lambda_{m_0}^{x_0}. \tag{5}$$

This equation is satisfied because the orders overlap spatially at the camera, in contrast to conventional cross-dispersed ES where channels are spatially separated. Typically, in the design of ES, it is mandatory that small portions of the spectrum appear duplicated at opposite sides on the camera for consecutive orders. This is required to avoid spectral gaps between consecutive orders. If the reference wavelength impinges the camera at x_1 for the order $m_0 + 1$, then the wavelengths at x_1 of order m are also known:

$$\lambda_m^{x_1} = \frac{m_0 + 1}{m}\lambda_{m_0}^{x_0}. \tag{6}$$

Considering Eqs. (5)-(6), it is possible to know two wavelengths per order, one at x_0 and the other at x_1. Now, the second hypothesis states that the dispersion curve for each order approximates by a linear function:

$$\lambda_m(x) = \lambda_{m_0}^{x_0}\frac{m_0\,(x_1 - x_0) + x - x_0}{m\,(x_1 - x_0)}. \tag{7}$$

From (7) the spectrometer is calibrated with a fairly good approximation from a single wavelength, as we will demonstrate below. In fact, the small discrepancies in the whole operational range ($400 - 850\,nm$) are equal or less than the spectral increment in one camera pixel. This large simplification enables to introduce the calibration wavelength in every spectral measurement achieving a self-calibrated ES. This calibration method is much more simple and robust than conventional ones. Moreover, a calibration to a second/third order can be achieved with our approach by just using another reference wavelength being still suitable for self-calibrated ES.

4. Experimental results

In this section we analyze the spectrum of different light sources demonstrating that the order sorting and the calibration process work properly for continuum and discrete spectral intensities. We show on Fig. 2(a) the CCD signal corresponding to the simultaneous detection of a white-LED source and a stabilized He-Ne laser emitting at 632.81 nm used as the calibration source. Equation (3) describes the CCD signal. Each column along the y-axis in Fig. 2(a) is the addition of wavelength-dependent periodic intensity patterns, each one from each diffraction order, producing an oscillatory behavior with periodic visibility. Maximum visibility is reached at y-points where the intensity patterns add in phase.

The Fourier transformation of the signal along the y-axis for each position x is shown in Fig. 2(b). This figure is described by (4). The orders are clearly resolved in the reciprocal space as expected by our proposal. Drawn over Fig. 2(b) is the channel map, consisting in a set of red lines which identify the center position of each diffraction order. Using our arrangement we were able to separate 20 orders, from $m = 12$ to $m = 31$, covering the broad spectrum range $400 - 850\,nm$. We point out that the number of orders is solely limited by the design of the ES, no matter the method for order sorting. In fact, a cross-dispersed ES with identical characteristics would

Optics EXPRESS

spatially separate equal number of orders. Our proposal could be used in very high resolution ES having high number of orders.

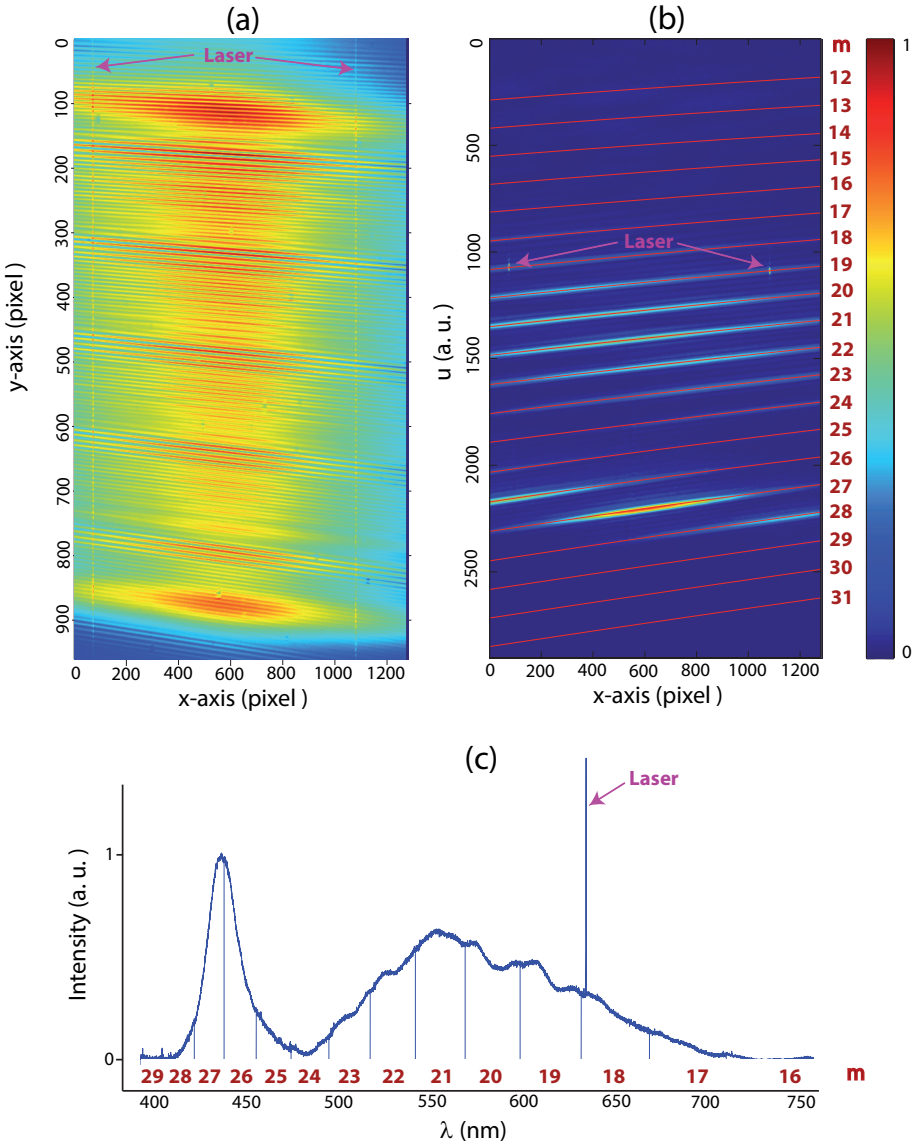

Fig. 2. (a) Signal recorded by the camera for simultaneous illumination with a white-LED source and a stabilized He-Ne laser. This signal is described by (3). (b) Fourier transformation (FFT) of the signal along the y-axis for each position x. This figure is described by (4). The red lines are the channel map indicating the center position of each diffraction order m. The self-calibration process is performed introducing in (7) the position x and order m of the laser peaks in (b). (c) Spectral intensity of the white-LED source by the addition of the intensity profiles along the channel map for orders 16 – 29.

Optics EXPRESS

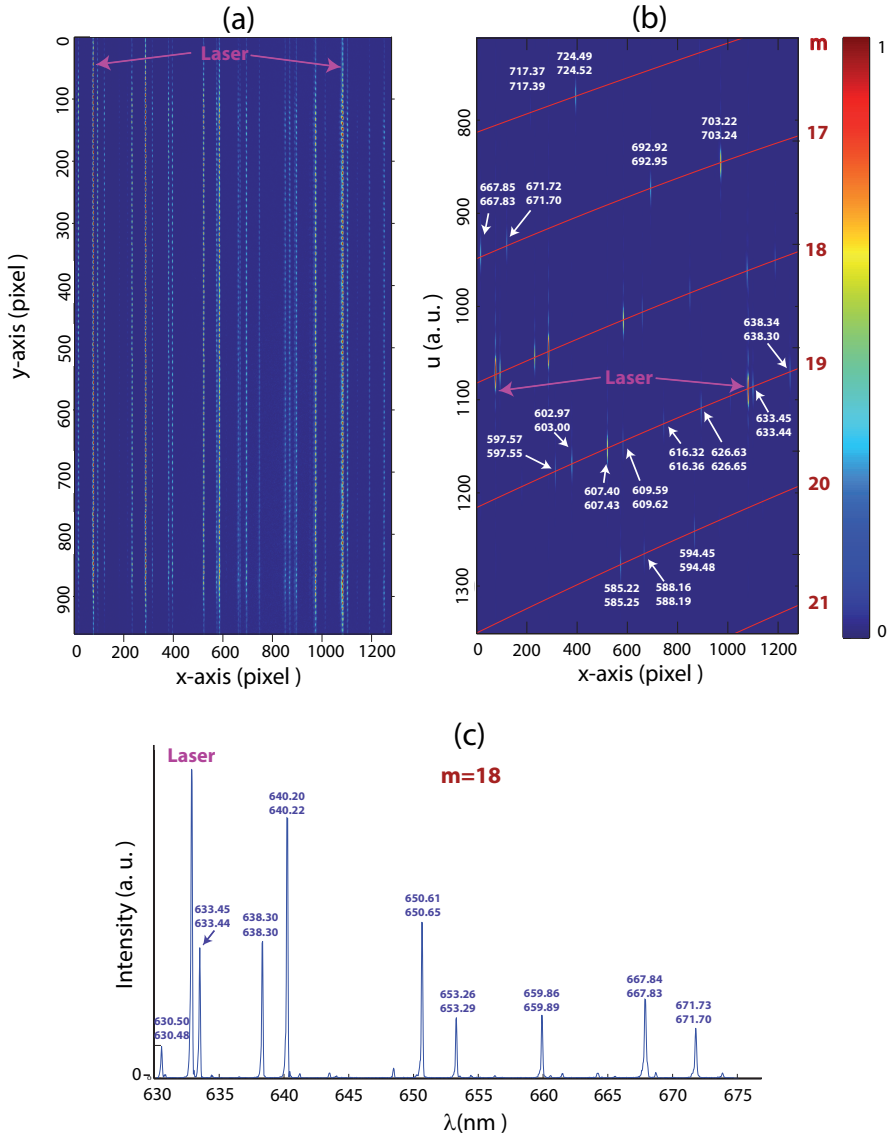

Fig. 3. (a) Signal recorded by the camera for simultaneous illumination with a Ne discharge lamp and the stabilized He-Ne laser. This signal is described by (3). (b) Fourier transformation (FFT) of the signal along the y-axis for each position x. This figure is described by (4). The red lines are the channel map indicating the center position of each diffraction order m. The self-calibration process is performed introducing in (7) the position x and order m of the laser peaks in (b). (c) Intensity profile along the channel $m = 18$. The numbers in (b)-(c) are the wavelengths in nm found with our method (top) and in [12] (bottom).

The calibration process is performed with the He-Ne laser. This wavelength is recorded together with the spectral intensity of the light source under study, as shown in Fig. 2(a). The Fourier transformation of the laser signal gives two peaks at $x_0 = 78$ for $m_0 = 18$ and $x_1 = 1079$ for $m = 19$, see Fig. 2(b). Introducing these values in (7) the spectrometer is self-calibrated. So, the spectral intensity of the white-LED source is the joint representation of the intensity profiles along the channel map corresponding to orders $16 - 29$, as shown in Fig. 2(c). Notice that each

Optics EXPRESS

channel covers a different spectral bandwidth giving by (7) and represented on the bottom of this figure. In order to avoid spectral gaps between consecutive orders the spectral information from consecutive orders at opposite sides on the CCD must be duplicated, as we said before. This redundant information is suppressed on the representation of Fig. 2(c).

The result from a discrete spectrum emitted by a Ne discharge lamp is shown in Fig. 3. The recorded image is composed of narrow periodic intensity patterns along the y-axis [Fig. 3(a)] at different positions x. This behavior is described by (3). The Fourier transformation of the signal along the y-axis for each position x [Fig. 3(b)] is described by (4). As expected, *sinc* functions along u at discrete positions x are obtained, each one centered at a specific order as it can be seen by adding the channel map in Fig. 3(b). In order to highlight the spectral details, we only show orders $16 - 21$ because their large intensities. The calibration is performed identically to that in Fig. 2 obtaining spectral values displayed (in nm) on the top position at each peak in Figs. 3(b). For comparison purposes the values found in [12] are displayed on the bottom showing that the spectral lines differ from tabulated values at most $0.04\,nm$. This difference is close to the spectral increment between consecutive pixels on x, which is the maximum accuracy that any calibration method can reach considering the discrete nature of the pixels. This proves the correctness of the self-calibration method.

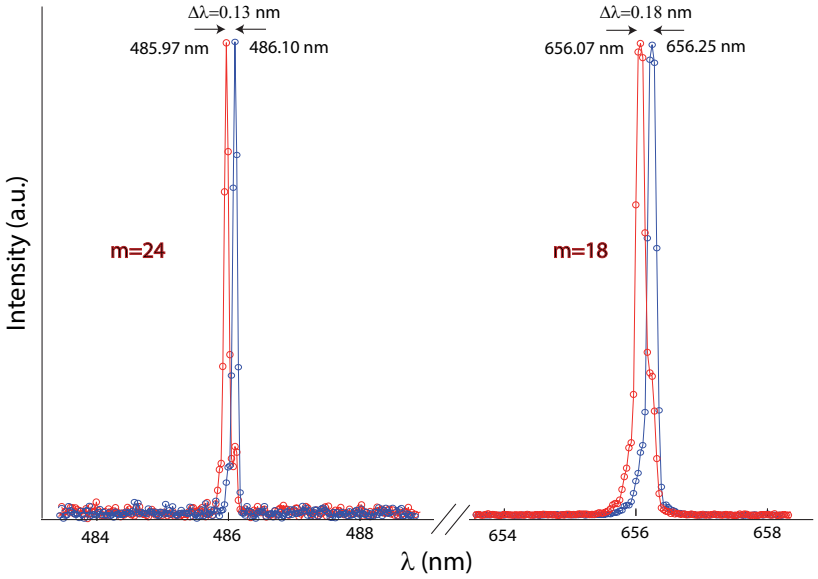

Fig. 4. Spectral intensity of a Hydrogen (blue) and deuterium (red) discharge lamps measured and self-calibrated independently. The optical setup has been subjected to moderate mechanical vibrations prior to measuring. The typical spectral shift in the green ($\Delta\lambda \sim 0.129\,nm$) and red ($\Delta\lambda \sim 0.176\,nm$) parts of the spectrum is resolved for the Hβ ($m = 24$) and Hα ($m = 18$) emission lines.

A detailed analysis of the spectrum for order $m = 18$ is shown in Fig. 3(c), where well defined individual peaks are obtained at the correct positions. The full wide at half maximum (FWHM) of each spectral line, $\Delta\lambda_{FWHM} \sim 0.09\,nm$, extends 3-4 pixels. This is used to find the resolving power, R, of our approach $R = \lambda/\Delta\lambda \sim 5000 - 7000$. These values are close to the greatest resolving power ($R_{max} \sim 10000$) reached for a ES with the characteristics analyzed here. In fact, R_{max} is calculated for spectral lines with FWHM that extends two pixels. Nevertheless, the found R-value is identical to the obtained for a cross-dispersed ES of the same characteristics. Our approach is not limited to this resolving power being possible to obtain very high resolving

Optics EXPRESS

capabilities for a proper ES design. It is also possible to numerically increase the resolving power of the ES using the point spread function (PSF) of the system. In [10] it is described a method to determine the PSF and to increase the resolving capabilities more than one order of magnitude. This process applied to our approach will be investigated in further research. It is important to note that the ES exhibits spectral line curvature, refereed as smile effect [13]. This is a common spatial distortion on the monochromatic image of the slit caused by the grating or by optical aberrations of the spectrometer elements. The smile effect curvature has been measured for the He-Ne laser and it has been assumed invariant in the whole operational range of the ES. This assumption allows to digitally correct the image in a simple manner before performing the Fourier transformation. Figures 2(a) and 3(a) are the images digitally corrected, the last one composed of straight vertical lines which indicates the correctness of the method to compensate the smile effect.

Finally, in order to show the advantages of the self-calibration process, we expose the ES to vibrations prior to measuring. These exaggerating environmental conditions try to simulate the spectral drift in a non-isolated experiment dealing with very high spectral resolution. Under these adverse conditions we evaluated the approach capabilities to distinguish very similar spectra emitted by a hydrogen (blue line) and a deuterium (red line) discharge lamps shown in Fig. 4. Each discharge lamp has been self-calibrated separately but their spectra are displayed together. The scale in the abscissa display a portion of orders 24 and 18 in which the most intense emission lines are localized. The spectral shift between the hydrogen and deuterium emission around the Hβ ($\Delta\lambda \sim 0.129\,nm$) and H$\alpha$ ($\Delta\lambda \sim 0.176\,nm$) is observed in agreement to [12] even under mechanical perturbance. In this particular case the calibration curves are shifted by a few pixels in the CCD. If the self-calibration is not applied, as in conventional echelle spectrometers, the spectrum of the hydrogen will roll at the opposite site of the deuterium spectrum giving wrong results. This last experiment shows that the self-calibration method works properly to resolve slightly spectral differences in a non-isolated ES, even in adverse environmental conditions. The application of this method largely reduce the isolation constrains enabling this technology to be portable and accessible to modest budgets.

5. Conclusions

A non-isolated self-calibrated high resolving power ($R \sim 5000 - 7000$) echelle spectrometer operating in a broad wavelength range ($400 - 850\,nm$) is demonstrated and experimentally performed. The order sorting takes place in the reciprocal space exploiting the properties of structured illumination. This design allows a very simple calibration method by using a single reference wavelength that can be implemented in every spectral measurement. Our approach is suitable for the development of self-calibrated echelle spectrometers without tricky and expensive stabilization methods to compensate spectral drifts due to environmental conditions. The overall process is simple, robust and fast. These important features open possibilities to a new family of non-isolated self-calibrated ES with moderate, high and very high spectral capabilities at competitive prices.

Funding

Ministerio de Economía y Competitividad (TEC2014-57394-P) and Consejo Nacional de Investigaciones Científicas y Técnicas (CONICET) (PIP 112-201501-00435).

Acknowledgments

P. V. acknowledges CNPq (Brasil). Carolina Rickenstorff gratefully acknowledges the CONACyT posdoctoral grant 266764. We thank J. A. Rodrigo and J. M. Soto for valuable discussions and advice.